The present thesis is based on the following papers:

PAPER I: Sohankar, A., Davidson, L. and Norberg, C., *"Numerical Simulation of Unsteady Flow Around a Square Two-Dimensional Cylinder"*, In Proc. 12th Australasian Fluid Mechanics Conference, R. W. Bilger (Ed.), pp. 517-520, The University of Sydney, Australia, Dec. 1995.

PAPER II: Sohankar, A., Norberg, C. and Davidson, L., *"Numerical Simulation of Unsteady Low-Reynolds Number Flow around Rectangular Cylinders at Incidence"* Journal of Wind Engineering and Industrial Aerodynamics, Vol. 69-71, pp. 189-201, 1997.

PAPER III: Sohankar, A., Norberg, C. and Davidson, L., *"Low-Reynolds Flow around a Square Cylinder at Incidence: Study of Blockage, Onset of Vortex Shedding and Outlet Boundary Condition"*, International Journal for Numerical Methods in Fluids, Vol. 26, pp. 39-56, 1998.

PAPER VI: Sohankar, A., Norberg, C. and Davidson, L., *"Simulation of Unsteady Three-Dimensional Flow around a Square Cylinder at Moderate Reynolds Numbers"*, Submitted for Journal publication.

PAPER V: Sohankar, A., Davidson, L., and Norberg, C. *"Application of Different Subgrid Scale Model in Large Eddy Simulation of Flow around a Square Cylinder", February 1998, Department of Thermo and Fluid Dynamics, Chalmers University of Technology, Gothenburg, Sweden.*

Contents

Abstract

The subject of flow past slender bluff bodies is of relevance to technical problems associated with energy conservation, structural design and acoustic emissions. The present work is restricted to an important sub-class of slender bluff body flow — the incompressible flow around a stationary cylinder having a rectangular cross section, the cylinder being exposed to a constant free stream velocity. Time-dependent two- and three-dimensional (2D/3D-) numerical simulations are carried out. Some useful quantities such as the dominant wake frequency (the Strouhal number), mean and RMS values of drag and lift, and various surface pressures etc. were calculated for different Reynolds numbers.

In 2D-simulations, the effects of cylinder side ratio (B/A, where B is the longest side) and flow incidence (α) were investigated. In these simulations an incompressible non-staggered arrangement SIMPLEC code was used. The QUICK and Van Leer schemes were used for the convective terms. The time discretization was implicit and a second-order Crank-Nicolson scheme was employed. The influence of Reynolds number ($Re \leq 500$), body side ratio ($B/A = 1 - 4$) and angle of incidence ($\alpha = 0^o - 90^o$) was investigated. Effect of the various numerical parameters such as time step, domain size, blockage, grid distribution and spatial resolution in both far- and near-body regions was investigated. At outlet of the computational domain, a convective Sommerfeld boundary condition was compared with a traditional Neumann condition. The onset of vortex shedding was investigated using the Stuart-Landau equation at various angles of incidence for a square cylinder.

In 3D-calculations, direct numerical simulation (DNS) of unsteady flow around a square cylinder at zero incidence for moderate Reynolds numbers ($Re = 150 - 500$) and large eddy simulation (LES) at $Re = 22 \times 10^3$ were performed. A non-staggered grid arrangement, incompressible, finite-volume code was used employing an implicit fractional step method with a multi-grid pressure Poisson solver. A second-order central scheme was used for the convective and diffusion terms. The influence of spanwise aspect ratio, finer grid and time step on the results were investigated for DNS. A study of transition from 2D to 3D flow, the wake structure, A- and B-mode of secondary vortices and a comparison of 2D and 3D results with experimental results were carried out in DNS simulations. Some dissimilarities with the flow around a circular cylinder were also investigated.

In LES simulations, three different subgrid scale models, the Smagorinsky, dynamic and dynamic one-equation models for $Re = 22 \times 10^3$, were applied and their results were compared with experimental results.

KEY WORDS: rectangular cylinders; incompressible flow; Reynolds number; numerical simulation; finite volumes; onset of vortex shedding; angle of incidence; blockage; outlet boundary condition; square cylinder; transition; DNS; LES

Acknowledgments

This work was carried out at the Department of Thermo and Fluid Dynamics, Chalmers University of Technology, Gothenburg, Sweden, under the supervision of Prof. Lars Davidson and Dr. Christoffer Norberg.

I would like to express my deep gratitude to Prof. Lars Davidson and Dr. Christoffer Norberg for our many discussions and their useful suggestions during the course of this research program. In addition, I would like to thank Christoffer for his careful proof-reading and for letting me profit by his knowledge of flow around cylinders.

I wish to acknowledge and thank the Ministry of Culture and Higher Education of I.R. of Iran for providing financial support during this work.

I also thank friends, colleagues and the staff of the Department for their great helps.

Last but not least, I express my deepest gratitude to my parents, wife and children for their support, patience and encouragement through the years.

Nomenclature

A	Shortest side of the cylinder, Paper 2 and 3
A	Computational aspect ratio of body, Paper 4 and 5
A_L	Instantaneous lift envelop amplitude
B	Longest side of the cylinder
B/A	Cylinder side ratio
C_D	Total drag coefficient
$C_{D'}$	RMS drag coefficient
C_{D_p}	Pressure drag coefficient
C_{D_f}	Friction drag coefficient
C_L	Total lift coefficient
C_F	Force coefficient $C_F = \sqrt{C_D^2 + C_L^2}$
C_{L_p}	Pressure lift coefficient
C_{L_f}	Friction lift coefficient
$C_{L'}$	RMS lift coefficient
C_M	Total moment coefficient
C_p	Pressure coefficient
C_{pb}	Base pressure coefficient at centerline
$C_{pb'}$	RMS base pressure coefficient at centerline
C_{ps}	Stagnation pressure coefficient
$C_{p,f}$	Surface averaged frontal side C_p
$C_{p,tb}$	Surface averaged top and bottom side C_p
C_S	The Smagorinsky constant
C	The constant in the Dynamic Model
C^k	The constant in the One-Equation Dynamic Model
d	Projected width in the streamwise direction ($= A\cos\alpha + B\sin\alpha$)
f_S	Shedding frequency
h	Projected length in the cross-stream direction ($= A\sin\alpha + B\cos\alpha$)
H	Height of computational domain
L_r	Time mean length of recirculating region
N_b	Number of nodes over one unit length of the cylinder surface
N_p	Average number of iterations per time step in the saturated condition
N_t	Average number of iterations per time step for the whole of the simulation
Re	Reynolds number, $U_\infty d/\nu$
Re_{cr}	Critical onset Reynolds number
Ro_{cr}	Critical onset Roshko number ($Ro = Re \times St$)

St	Strouhal number, $f_S d/U_\infty$
t	Non-dimensional time (scaled with d/U_∞)
U	Streamwise velocity
V	Cross stream velocity
W	Spanwise velocity
U_∞	Free stream velocity
$\bar{u}$, $\bar{v}$, $\bar{w}$	Cartesian components of resolved velocities (LES)
X_d	Extent of domain downstream of body
X_u	Extent of domain upstream of body
α	Angle of incidence, Papers 2 and 3
α	Modified Crank-Nicolson coefficient, Papers 4 and 5
β	Blockage parameter ($= d/H$)
δ	Minimum cell size adjacent to the body
Δ	Maximum cell size in far field
Δ_z	Cell size in the spanwise direction
Δt	Non-dimensional time step
ν	Kinematic viscosity
ν_t	Subgrid eddy viscosity
ν_r	ν_t/ν
ρ	Fluid density
ω	Modified Crank-Nicolson coefficient, Papers 4 and 5
Γ_x	Streamwise circulation
Γ_z	Spanwise circulation
$\langle\overline{u'u'}\rangle_t$	Spanwise-average of resolved streamwise Reynolds normal stress (LES)
$\langle\overline{v'v'}\rangle_t$	Spanwise-average of resolved cross-stream Reynolds normal stress (LES)
$\langle\overline{u'v'}\rangle_t$	Spanwise-average of resolved Reynolds shear stress (LES)
$\langle\overline{w'w'}\rangle_t$	Spanwise-averaged of resolved spanwise Reynolds normal stress (LES)
NBC	Neumann boundary condition
CBC	Convective boundary condition
SM	The Smagorinsky Model
DSM	The Dynamic Subgrid Model
$OEDSM$	The One-Equation Dynamic Subgrid Model

1 Introduction

Over the past hundred years or so, the flow around slender cylindrical bluff bodies has been a source of fascination and intricacy, and this flow situation has thus stimulated and attracted a vast amount of research studies. However, it was not until 1878, when Strouhal published his pioneer paper [21] on singing wires caused by vortex shedding, that this type of flow became a subject of quantitative research. This is mainly because of the engineering significance associated with energy conservation, structural design and acoustic emissions. For instance, fuel consumption in aircrafts and road vehicles might be decreased by reducing aerodynamic drag, and multi-story buildings such as skyscrapers ought to be designed so as to minimize convective heat loss and dust deposits. In addition, structures must be designed so as to avoid potentially disastrous wind-induced oscillations, and knowledge of vortex shedding characteristics is crucial in the design of vortex shedding flow-meters. Slender bluff body cross flow configurations arise in numerous industrial applications and environmental situations, e.g. flow-metering devices; cooling of electronic components and equipment; the obstructed spaces between co-rotating disks in magnetic disk storage devices; and tall buildings and other technical structures such as cooling towers, chimneys and suspension bridges. Bluff-body, induced-flow unsteadiness and mixing may also be used to enhance heat and mass transfer to or from the bluff body and/or its surroundings. Aside from motivations provided by the above practical factors, the unsteady flow and heat transfer associated with cylindrically shaped bluff bodies are interesting in their own right and have been the subject of considerable basic research. In these studies, the principal objective has mainly been to measure and/or calculate the field variables and related quantities from which to determine cylinder drag and lift coefficients as well as Strouhal and Nusselt numbers. The studies can be classified according to the number, arrangement and cross-sectional shapes of the cylinders, the character of the approaching flow and whether it is of a free-stream or confined type.

In general, the flow around bluff bodies contains many complex phenomena. The near wake of a bluff body is involved in the interactions between an attached shear layer on the frontal part of the body, the separating free shear layers springing from the sides of the body, and a massive wake flow downstream of the body, each with different and perhaps even coupled processes of developing instabilities as the Reynolds number is increased. A bluff body is one in which the flow under normal circumstances separates from a large section of the body surface thus creating a massive wake region downstream. Now consider a slender bluff body of constant cross-sectional area, i.e. a cylinder, exposed to a cross-flow with a constant free stream velocity, U_∞. An appropriate Reynolds number is then $Re = U_\infty d/\nu$, where d is the projected width of the cylinder in the streamwise direction. In this flow situation there are two free shear layers that trail aft in the flow bounding the wake region. Since the innermost portion of the free shear layers moves much more slowly than the outermost portion of the layers, which are in contact with free stream, the free shear layers tend to roll up into discrete, swirling vortices.

At this point, it may be suitable to draw attention to some characteristics in the flow around slender cylindrical bluff bodies as the Reynolds number is increased from about unity with Re based on the cross-stream dimension, the diameter. In general terms, the following short description applies to the flow around a circular cylinder. At low Reynolds numbers, say less than about 100, the description is believed also to be valid for the case under consideration, i.e. the flow around a rectangular cylinder. However, at higher Re, the sharp corners may play a significant role in the development of flow instabilities and other flow characteristics. At Reynolds numbers below about unity, the flow is fully attached with no separation. As Re is increased, the flow separates and a pair of steady symmetric vortices forms behind the body. For the circular cylinder, this happens at around $Re \approx 3.2 - 5$ [22, 24]. At higher Reynolds numbers, the formation vortex length of the recirculation region behind the body grows with increasing Re. At a critical onset Reynolds number ($Re = Re_{c1} \approx 50$), the twin-vortex arrangement becomes unstable, and a time-periodic oscillation wake and a staggered vortex street are formed. The separated vortices are "shed" alternately from the upper and lower side of the body. The periodic phenomenon is referred to as vortex shedding whereas the antisymmetric wake flow pattern is referred to as the von Kármán vortex street. This is the first 2D wake transition which is called Bénard-von Kármán instability [16]. This transition contains a 2D instability from a steady wake to a periodic wake. A non-dimensional shedding frequency is called the Strouhal number, in this context defined as $St = f_S d/U_\infty$. The near-wake flow unsteadiness gives rise to fluctuating drag and lift forces, which can stress the body by making it vibrate. Cylinder vibration can, among other things, (i) increase the vortex strength, (ii) increase the spanwise wake correlation and (iii) force the shedding frequency to match the vibration frequency (lock-in or synchronization)[2]. In addition, the associated fluctuating forces on the body, the alternate shedding of vortices, may cause structural vibrations, acoustic noise emissions (Aeolian tones) or, in some cases, resonance, which can trigger a failure of structures. By increasing the Reynolds number, a 3D transition is developed at around Reynolds number 200 (Re_{c2}), and the three-dimensional flow effects appear. Within the laminar régime, which is between these two instabilities ($Re_{c1} < Re < Re_{c2}$), the vortex shedding is characterized by a very well-defined frequency, which, when non-dimensionalized with the viscous time scale d^2/ν, exhibits an approximate linear increase with the Reynolds number [17, 19]. As Re increases still higher ($Re = 200$), the effects of flow three dimensionality and turbulence become more and more pronounced.

In recent years, the subject of flow around bluff bodies has received a great deal of attention as result of increasing computer capabilities and improvements in experimental measurement techniques. The vast majority of these investigations has been carried out for the flow around a circular cylinder whereas, from an engineering point of view, it is necessary to study flow around other bluff-body shapes such as sharp-edged rectangular cross-sectional cylinders. Structures that typically have rectangular or near-rectangular cross-sections include architectural features

on buildings, the buildings themselves, beams, fences and occasionally stays and supports in internal flow geometries. Except perhaps for the circular cross-section, detailed knowledge of the unsteady flow field around cylinders is rather limited owing to the considerable effort involved in taking unsteady measurements and calculations in such flows. Consequently, there is a considerable gap of knowledge for flow around rectangular cylinders concerning to the effects of flow incidence at various Reynolds numbers and for different cross-section geometries and different wake transition processes. Thus, one objective of this thesis is to fill this gap. Another objective is a better understanding of the different instabilities of the vortex shedding phenomenon.

2 Problem Under Consideration

The problem under consideration in Papers 1-3 is depicted in Fig. 1(a). A fixed rectangular cylinder with a side ratio of B/A, where B is the longest side of the cylinder, is exposed, at some angle of incidence α, to a constant free stream velocity, U_∞.

The problem under consideration (Papers 4-5) is described in a Cartesian coordinate system (x, y, z), in which the x-axis is aligned with the inlet flow direction, the z-axis is parallel with the cylinder axis and the y-axis is perpendicular to both these directions, as shown in Fig. 1(b). A fixed two-dimensional square cylinder with a side d ($B/A = 1$, $\alpha = 0^o$) is exposed to a constant free stream velocity, U_∞.

In this study, all dimensions are scaled with the projected width of the cylinder in the streamwise direction, $d = A\cos\alpha + B\sin\alpha$ ($0^o \leq \alpha \leq 90^o$). Scaling with d also applies to Reynolds and Strouhal numbers, $St = f_S d/U_\infty$, where f_S is the shedding frequency. The vertical distance between upper and lower walls, H, defines the solid blockage of the confined flow (blockage parameter $\beta = 1/H$). Velocities are scaled with U_∞ and physical times with d/U_∞. Forces and moments acting on the cylinder are scaled with d and the dynamic pressure of the upstream flow, $\rho U_\infty^2/2$. Pressure coefficients are defined as $C_p = 2(p - p_\infty)/\rho U_\infty^2$, where p_∞ is the static pressure of the upstream flow. Calculated pitching moments are referred to the geometrical center with positive values in the clockwise direction. The origin of force coordinates is placed at the geometrical center with drag force, D, positive in the x-direction and lift, L, positive in the y-direction, see Fig. 1. The relevant computational parameters of the present study are summarized in Table 1.

3 Boundary Conditions

A uniform flow ($U = 1$, $V = W = 0$) was prescribed at the inlet, which is located X_u units upstream of the cylinder. At the outlet, which is located X_d units downstream of the body, the Neumann ($\frac{\partial U_i}{\partial x} = 0$, Papers 1-3) and the convective boundary condition ($\frac{\partial U_i}{\partial t} + U_c \frac{\partial U_i}{\partial x} = 0$, Papers 3-5) were used for all velocity components. The value of U_c was set equal to U_∞. No-slip

Paper	$2D/3D$	Re	α (^{o})	B/A	H	X_u	X_d	Δt
I	2D	45-250	0	1	14-50	7.5-18	10-56	0.02-0.05
II	2D	≤ 200	0-90	1-4	20	10,20	26,40	0.025 (0.0125)
III	2D	45-200	0-45	1	20 (40)	10	3-26	0.025
IV	2D,3D	150-500	0	1	18	8.5	12.5	0.025(0.0125)
V	3D	22000	0	1	16	7	16	0.025

Table 1: Summary of computational parameters. α=angle of incidence, H = Height of computational domain, X_u = Distance from body to inlet, X_d = Distance from body to outlet, B/A = Side ratio of cylinder (A and B are the shortest and longest sides of the body, respectively)

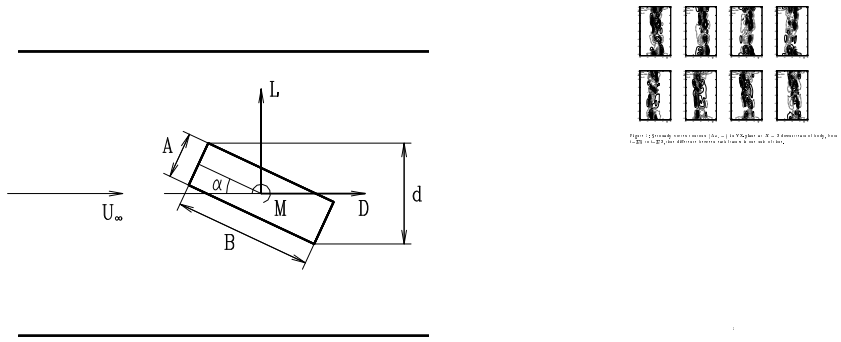

(a) (b)

Figure 1: Flow configurations of the present study. (a) Paper 1-3, (b) Paper 4-5.

conditions ($U = V = W = 0$) were prescribed at the body surfaces. Symmetry conditions simulating a frictionless wall were ($\frac{\partial U}{\partial y}$=$\frac{\partial W}{\partial y} = V = 0$) used at the upper and lower boundaries. A periodic boundary condition (Papers 4-5) was used in the spanwise direction. The normal derivative for the pressure was set to zero at all boundaries. The second normal derivative (Papers 1-3) and normal derivative (Papers 4-5) for the pressure are set to zero at all boundaries.

4 Numerical Details

The time-marching calculations started with the fluid at rest and continued with a constant time step Δt, see Table 1. During the iterative sequence, convergence was assessed at the end of each iteration on the basis of the residual sources criterion, which compares the sum of the absolute residual source over all the control volumes in the computation field for each finite-volume equation and pressure. The residuals for the continuity and momentum were normalized with the incoming mass flux and momentum flux, respectively. The convergence criterion was set to

0.001 Test in 2D- and 3D-simulation with convergence criterion of 0.0001, and double precision showed no significant changes in the results whereas the number of iterations for convergence increased approximately two times.

The grid distribution is uniform with a constant cell size, Δ, outside a region from the body which extends a number of units upstream, downstream and sideways (in the x- and y-directions). The distance from the cylinder surface to the nearest grid point defines δ. The hyperbolic tangent function was used for stretching the cell sizes between these limits (δ and Δ). For example, the gird used for LES simulations is shown in Fig. 2 for the stretching region and the whole of the calculation domain. At this point, it is worth mentioning why the hyperbolic tangent function is used for stretching points in non-uniform grids. As is discussed by Thompson *et al.* [23], the truncation error is strongly affected by the distribution of points in non-uniform grids. They reported that the best choices for stretching points are the hyperbolic tangent and the hyperbolic sine functions when the variation of spacing is large. The hyperbolic sine gives a more uniform distribution in the immediate vicinity of the minimum spacing, and thus has less error in this region, but the hyperbolic tangent has the better overall distribution. The important point is that the spacing must not be allowed to change too rapidly in high gradient regions. After some testing for the present study, it was decided to use the hyperbolic tangent with a non-uniform grid extending some units upstream, downstream and sideways from the body.

In 3D-simulations, in the spanwise direction (z-direction, Papers 4-5), a uniform grid with a distance of Δ_z between nodes was used.

The fundamental stability condition of explicit schemes is that the convection Courant Number, CFL ($U\ \Delta t\ /\Delta x$) should be smaller than one. By calculating CFL in the x- and y-directions for the present study, it is found that the regions where CFL is higher than one, are located very close to the body where a very fine grid must be used. However, at a short distance from the body, the condition of $CFL \leq 1$ is satisfied. In the present study, the geometry of the problem under consideration contains sharp corners, and thus the rapid variation in flow variables in the vicinity of of corners requires a very fine grid (Fig. 2). To satisfy the stability condition, when using explicit schemes and for such grids, the computational time step (Δt) would normally attain unacceptable low values. From this point of view it is thus preferable to use *implicit* methods for which there are no conditions on numerical stability. However, for accuracy, the CFLs should not exceed one too much.

More information on the numerical details is found in Papers 1-5.

5 The Numerical Procedure

In this thesis, two different finite-volume codes are used with some adaptation for the present simulations. The first code, which is used in Papers 1-3, is briefly described in the following.

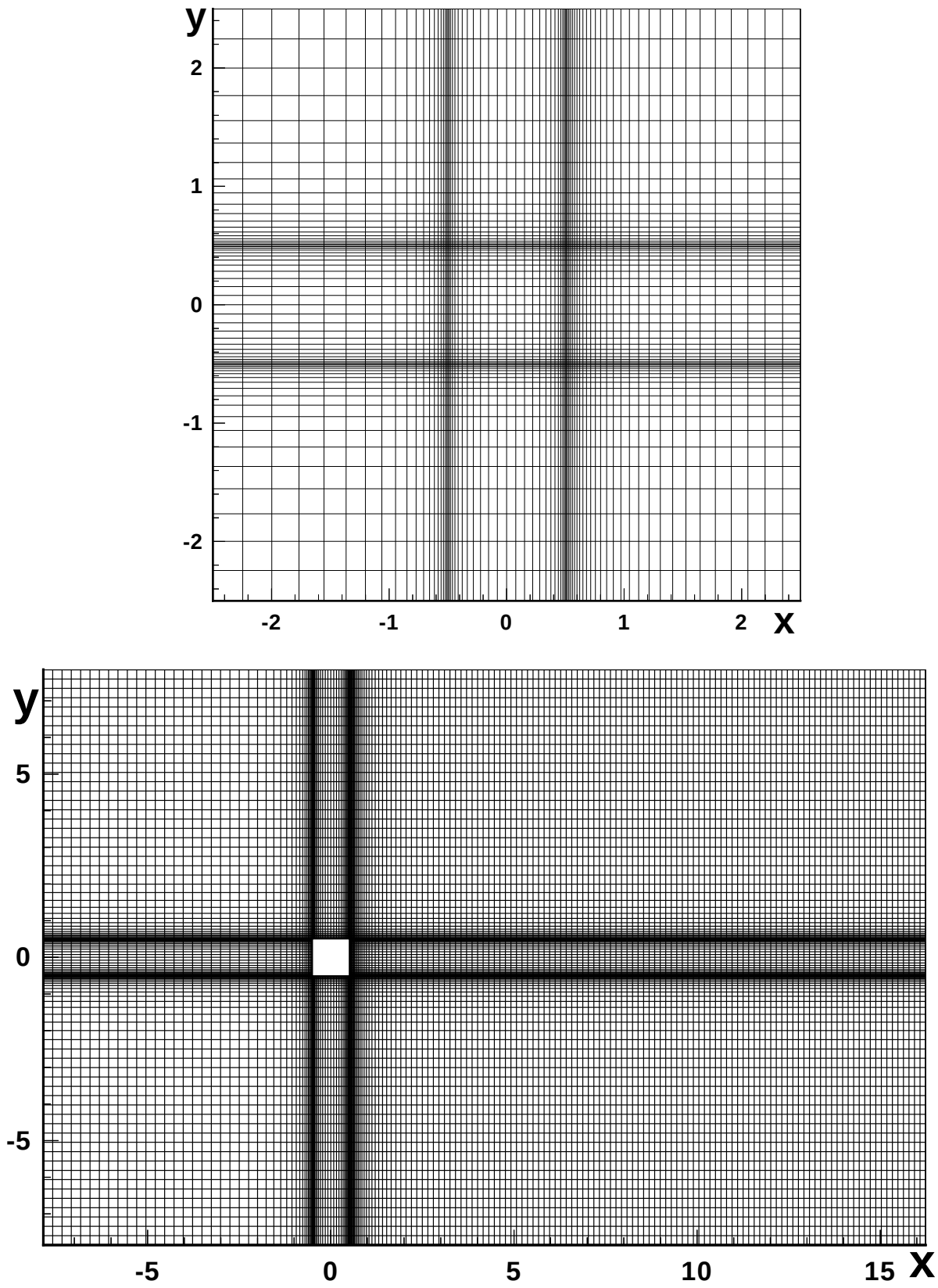

Figure 2: The non-uniform grid on the xy-plane (Paper 5). Top: 73×63 grid in the stretching region, Bottom: 185×105 grid in the whole domain. The body is located at $x \in (-0.5, 0.5)$, $y \in (-0.5, 0.5)$.

This is an incompressible SIMPLEC[15] finite volume code, CALC-BFC (Boundary Fitted Coordinates)[3], employing a non-staggered grid arrangement. The scheme is implicit in time, and a Crank-Nicolson scheme of second order was used. The convective terms were discretized using either the third-order QUICK differencing scheme [9] or the second-order scheme of Van Leer [7, 8]. The diffusive terms were discretized using central differencing. More details on the code and equations are given in Ref. [3].

The second computational code was used in Papers 4 and 5. In this code, a non-staggered grid arrangement in an incompressible finite-volume code was used, employing an implicit fractional step method with a multigrid pressure Poisson solver. A second-order central scheme was used for the convective and diffusion terms. All terms in the momentum equation were advanced in time using the modified Crank-Nicolson method with variable coefficients. More details on the code and equations are given in Papers 4 and 5.

6 Summary of papers

6.1 Paper 1

This Paper reports calculations of two-dimensional unsteady flow of vortex shedding past a square cylinder, at $Re = 45 - 250$ and zero angle of incidence. The influence of the location of the inflow, outflow and side walls (blockage), respectively were investigated at $Re = 100$. The onset of vortex shedding was predicted between $Re = 50$ and $Re = 55$. The fully developed flow at $Re \geq 55$ exhibited a well-defined vortex shedding frequency. When using the RMS lift coefficient as an indicator, a strong sensitivity to various numerical parameters was demonstrated. Recommendations for the required size of the domain, grid distribution, time step and spatial resolution in the near-body region are given ($Re = 100$). A number of quantities such as lift and drag coefficients, various surface pressure coefficients and the mean vortex formation length behind the body were calculated for different Reynolds numbers. Observations of instantaneous streamlines revealed that the separation, in fully developed flow, occurred predominantly from the rear corners at $Re \leq 125$ and predominantly from the upstream corners, as the vortex shedding became more powerful, at higher Re. When separation was located at the upstream corners, the flow in the separation bubble on the sides created a near-wall flow directed upstream. With increasing strength of the shedding process, this effect presumably becomes more pronounced.

The blockage effect, which can be qualitatively described as an effective increase in the oncoming free stream velocity, on the Strouhal number was also investigated by using a third-order QUICK [9] scheme and a second-order Van Leer scheme. This comparison shows that the Strouhal number increases with increasing blockage for both schemes, see Fig. 3, although the results for the QUICK [9] scheme had better agreement with experimental results. At these relatively low blockages, the blockage behavior is similar to what is normally found at much higher Reynolds numbers (in turbulent flow), where the Strouhal number is more or

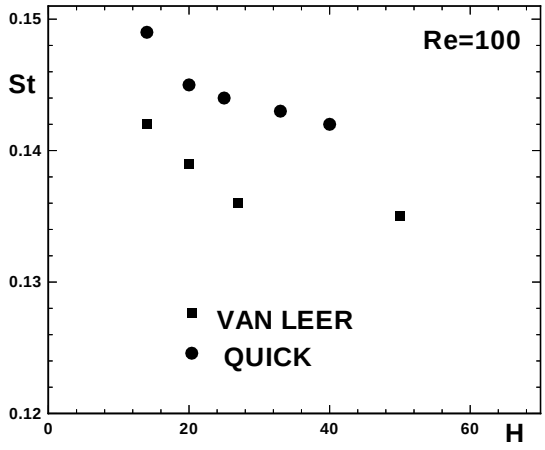

Figure 3: The effect of blockage ($\beta = 1/H$) on Strouhal number

less independent of the Reynolds number. In the blockage effect study, it was observed that, at blockages less than 3%, when using the QUICK [9] scheme, the calculations exhibited a few unphysical oscillations. Further investigations, which were carried out in Paper 2 and Paper 3, show that unphysical oscillations are caused by too coarse grid in the far field of the computational domain. The unbounded QUICK [9] scheme is more sensitive to coarse grids than is the bounded Van Leer scheme.

6.2 Paper 2

In this paper, calculations of unsteady 2D-flow around rectangular cylinders at incidence were performed for $Re \leq 200$. The influence of the cylinder side ratio ($B/A = 1-4$) at various angles of incidence ($\alpha = 0^o - 90^o$) was investigated. The results are in reasonable agreement with the indeed scarce experimental data available at these low Reynolds numbers, see e. g. Figs. 4 and 5 for Strouhal number and drag coefficient.

From Paper 1 and later analysis in this paper, for $B/A = 1$ and $\alpha = 0^o$ ($\beta = 5\%$), it is found that that the separation for $Re \leq 100$, at all times in the fully saturated state, occurred from the rear corners, predominantly from the rear corners at $Re = 125$, with occasional upstream corner separation, predominantly from the upstream corners at $Re = 150$, and, finally, at all times, from upstream corners for $Re \geq 175$. This is in reasonable agreement with Franke *et al.* [4], who report separation from upstream corners for $Re > 150$ ($\beta = 8.3\%$).

As is seen in Fig. 4, at $Re = 100$, the Strouhal number (St) decreases smoothly by projected side ratio, while, for $Re = 200$, it increases rather abruptly at around $h/d = 1.5$. At $h/d \geq 2$ for $Re = 200$, the flow reattaches on the longest side, which not is the case at $h/d < 2$. For $Re = 100$ at all side ratios investigated, separation points are located at the leeward corners,

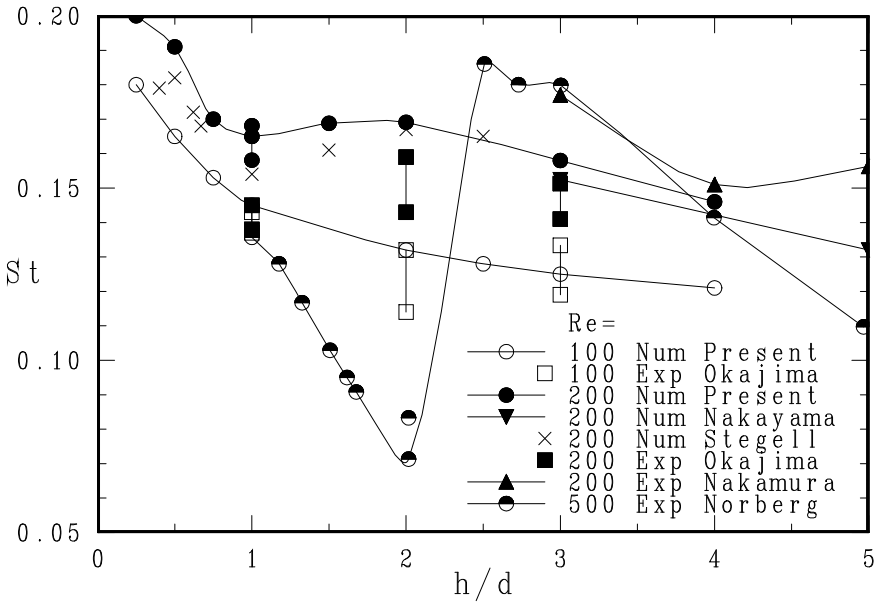

Figure 4: Strouhal number *vs.* projected side ratio.

while, at $Re = 200$, these points are located at the windward corners with back-flow occurring at the side surface. Up to $h/d = 1$, this back-flow covers the whole surface but, by increasing the side ratio, attachment points appear at the side surfaces, which causes a small jump in St, see Fig. 4. At $h/d = 2$, these attachment points are located near the leeward corners with subsequent separation. In terms of the diameter, d, the reattachment lengths at $h/d = 3 and 4$ are approximately the same as for $h/d = 2$. At $h/d = 1.5$, the mean flow is nearly but not fully reattached. Thus the critical length for reattachment seems to be between $h/d = 1.5$ and $h/d = 2$. At this $Re = 200$, in agreement with [20], there is no spectacular jump in St as is found at higher Re in turbulent flow, see e.g. $Re = 500$ in Fig. 4. For both Strouhal number and RMS lift, local extreme values were indicated at this critical length. The experiments in Nakamura *et al.* (1994) [11] indicate $Re \simeq 250$ as the critical Re for the appearance of a jump in St. In their experiments, however, the emphasis was on elongated cylinders with $h/d = 3 - 16$. Nevertheless, their Strouhal numbers at $h/d = 3$ and 4 are in good agreement with the present data, see Fig. 4. Interestingly, there was no indication of a local maximum in the drag coefficient or base suction coefficient at some intermediate critical side ratio, see Fig. 5. In turbulent flow, such a maximum occurs at around $h/d = 0.6$, see e.g. [1, 12].

This study also shows that the behavior of all quantities at low angles of incidence (approx. $\alpha < 20^o$) and at high angles (approx. $\alpha > 70^o$) is significantly different from that in between these regions. This is a consequence of fundamentally different evolutions of flow features close to the cylinder. The mechanism of vortex shedding in these regions is shown for one case, $Re = 200$, $B/A = 4$, $\alpha = 15^o$, in Figs. 6 and 7. The figures show instantaneous streamlines, and

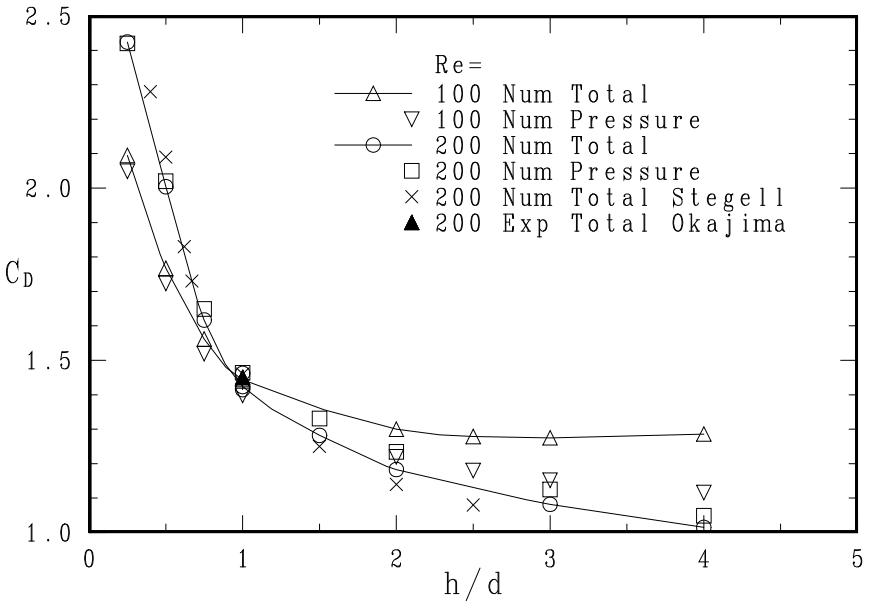

Figure 5: Mean drag coefficients *vs.* projected side ratio.

pressure and vorticity contours for eight instances in one period of vortex shedding, which are marked $1-8$ corresponding to eight instances in one period of vortex shedding as are seen in the time history of the lift and drag coefficients. In these frames, the direction and the magnitude of resultant forces are shown by vectors, and attachment and separation points are labeled A and S, respectively. At low angles of incidence, especially at high side ratios, an anti-clockwise secondary vortex forms somewhere on the leeward upper surface, e.g. see frames 1 and 8 in Fig. 6. It is then pushed by the vortex which forms at the windward upper corner and rolls it down on the leeward upper surface. When the secondary vortex reaches to the leeward lower corner, this vortex merges with another vortex formed at the windward lower corner and is finally shed in the wake flow, see frames 1 to 6 in Fig. 6.

Apart from the physical parameters investigated, i.e. Reynolds number, body side ratio and angle of incidence, it was found that the results were also strongly dependent on various numerical parameters, such as time step, domain size and spatial resolution in both the far- and near-field. Some of the discrepancies between the present results and those of previous numerical studies must be attributed to differences in the above mentioned numerical parameters. When using the RMS lift coefficient as an indicator, a strong sensitivity to various numerical parameters was demonstrated.

6.3 Paper 3

This paper presents calculations of unsteady 2D-flow around a square cylinder at incidence ($\alpha = 0^o - 45^o$) for different Reynolds numbers ($Re = 45 - 200$) using two kinds of outlet

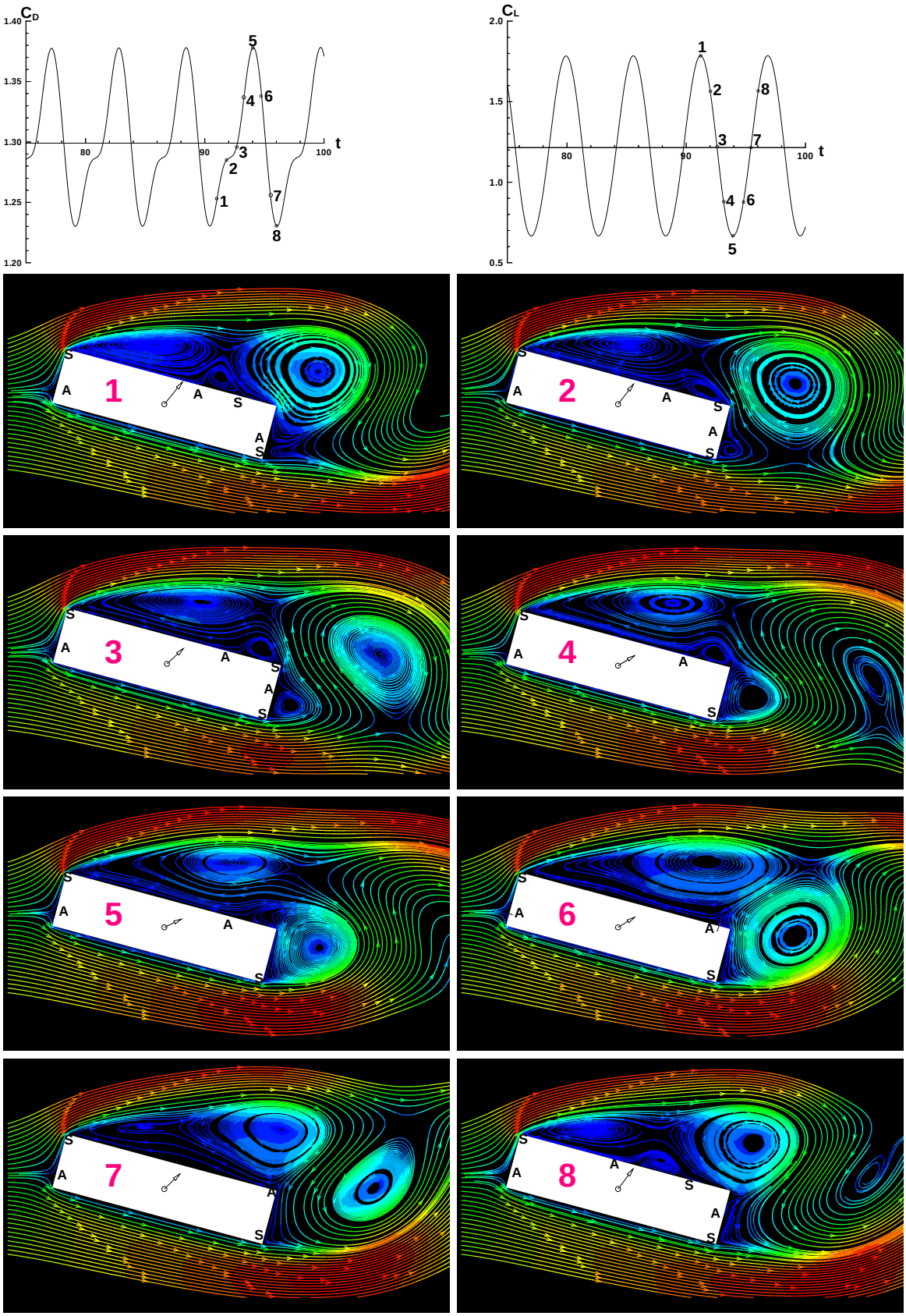

Figure 6: Top: Time history of drag and lift coefficients; Bottom: Instantaneous streamlines in eight instances during one period of vortex shedding. $Re = 200$, $B/A = 4$, $\alpha = 15^o$. Please note that the streamlines are colored by the velocity magmitude, $\sqrt{U^2 + V^2}$.

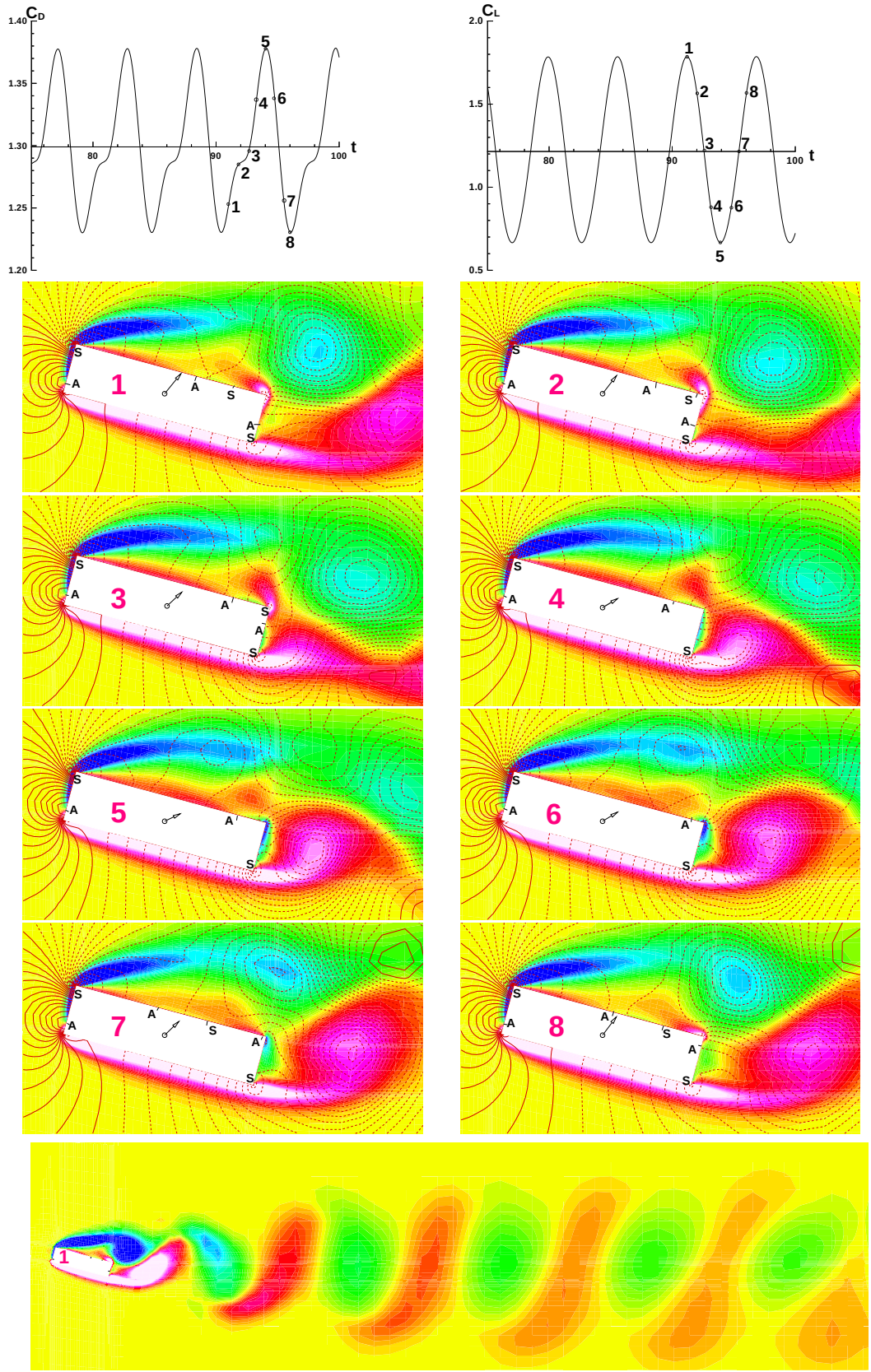

Figure 7: Top) Time history of drag and lift coefficients; middle) Time sequence of vorticity contours(color: yellow zero vorticity) and pressure contours(lines, solid:positive and dash:negative) Bottom) vortex shedding for maximum lift (frame 1). $Re = 200$, $B/A = 4$, $\alpha = 15^o$

boundary conditions.

At the outlet of the computational domain, a convective Sommerfeld boundary condition is compared with a traditional Neumann condition. It is found that the Neumann boundary condition generates disturbances in the upstream flow which are evidently damped out rather slowly. This causes the number of iterations per time step (N_{it}) to increase, especially in comparisons with convective boundary condition, see Fig. 8. The number of iterations per time step is a measure of the CPU time of the calculation. Thus, there was a significant savings in CPU time with the use of the convective boundary condition. In general, the convective boundary condition is shown to be more effective in reducing CPU time in three different ways; (i) by decreasing the number of iterations for convergence in each time step, (ii) by decreasing the CPU time for each iteration owing to a reduction reduced the necessary downstream extent of the domain and, finally, (iii) by decreasing the time to reach fully periodic flow.

In Paper 1, for the square cylinder at zero incidence, the blockage effect was investigated for $Re = 100$ and $\Delta = 0.7$, far-field resolution, using two different schemes for the convective terms (QUICK, Van Leer). In that study, it was reported that the calculations exhibit unphysical oscillations for blockage less than 3% when using the QUICK scheme. For the reduction of truncation errors and numerical diffusion, which are more severe in non-uniform grid simulations, the results of Paper 2 as well as this study point to the special importance of a suitable grid distribution and a sufficiently fine far-field resolution. In this study, by decreasing blockage to 2.5% for different Reynolds numbers, the effect of blockage was investigated. Since both grid distribution and far-field resolution were changed in this study, in comparison with Paper 1, we could not detect any unphysical oscillations in the present calculations. When changing the blockage parameter from $\beta = 5\%$ to $\beta = 2.5\%$, the strongest effects occurred for the base suction coefficient. For $Re = 100$, 150 and 200, the decrease in base suction was 7.6%, 5.4% and 5.0%, respectively. The corresponding changes in other quantities were rather small (less than 3%). These changes are all similar to an increase in the Reynolds number corresponding to the fact that an increase in blockage is effectively an increase in the oncoming velocity.

At least for the non-uniform grids employed in this investigation and for such low-Reynolds number vortex shedding flows ($45 \leq Re \leq 200$), it is recommended that the cell Reynolds number (Re based on far-field resolution Δ) be less than 30 for obtaining results that are independent of grid.

The onset of vortex shedding is investigated using the Stuart-Landau equation, at various angles of incidence and for a solid blockage of 5%. For the full range of possible incidences, i.e. $0^o \leq \alpha \leq 45^o$, the onset of vortex shedding occurred within the interval of $40 < Re_{cr} < 55$, with a decrease in Re_{cr} with increasing α, see Fig. 9. Using a procedure based on the linearized Stuart-Landau equation, at a blockage of 5%, individual critical values at some selected incidences were calculated. For instance, at incidences $\alpha = 0^o$ and 45^o, the onset values were $Re_{cr} = 51.2 \pm 1.0$ and 42.5 ± 1.0, respectively.

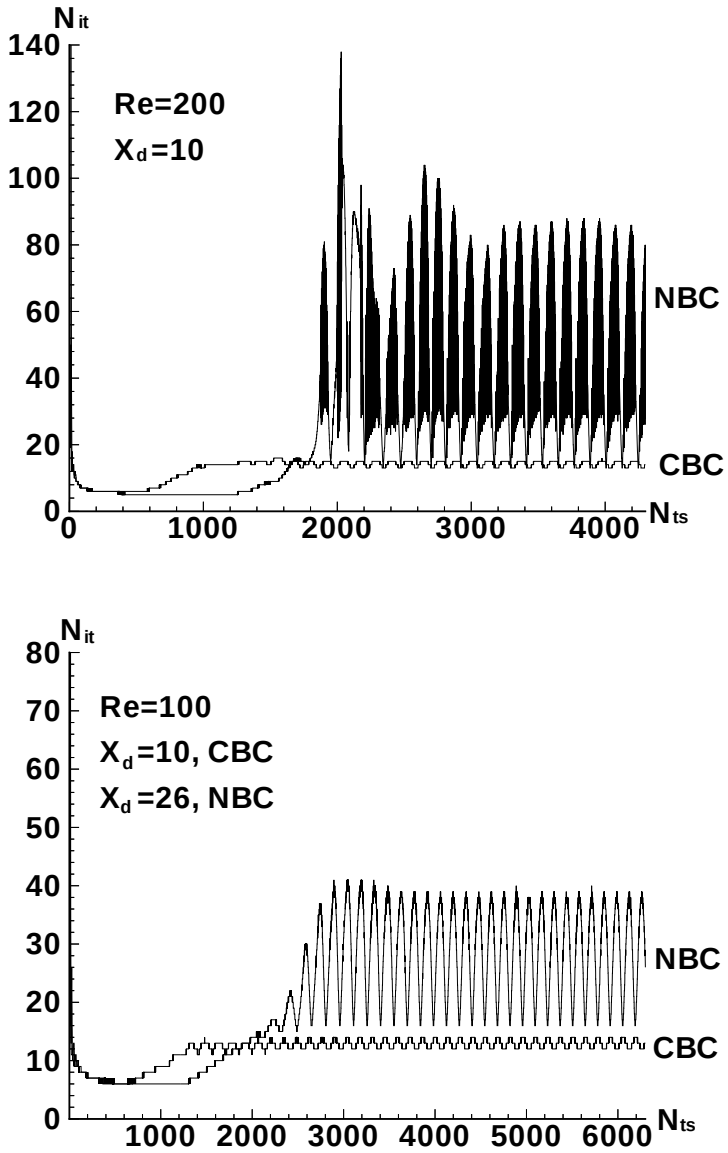

Figure 8: Time evolution of the number of iterations (N_{it}) per time step for the Neumann (NBC) and convective outlet boundary conditions (CBC), ($Re = 100, 200$, $\alpha = 0^o$). N_{ts} and X_d are the time step number and distance from body to outlet, respectively.

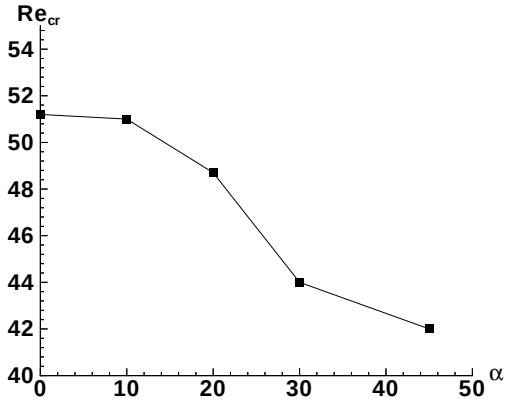

Figure 9: Critical Reynolds number for different angles of incidence.

This study also shows that the behavior of quantities such as the Strouhal number and the lift and drag coefficients at low angles of incidence (particularly, $\alpha \leq 20^o$) is different from fully separated flow at higher angles of incidence (approximately $\alpha > 20^o$). By considering the moment coefficient (C_M) *vs.* α for different Reynolds numbers, it is seen that the slope of C_M close to zero incidence is negative ($\partial C_M/\partial\alpha < 0$). As the turning moment was defined as positive in the clockwise direction, this means that the square cylinder within this range of Re, as also for much higher values of Re [12], has a stable posture.

6.4 Paper 4

Direct numerical simulations were carried out of 2D and 3D unsteady flow past a square cylinder at zero incidence (flat face facing the flow) at moderate Reynolds numbers ($Re = 150 - 500$) and for a solid blockage of $\beta = 5.6\%$. Some useful physical quantities, such as the dominant wake frequency (Strouhal number), mean and RMS values of lift and drag, were computed. The influence on the results of the spanwise aspect ratio using periodic boundary conditions and finer grid and time step are also investigated. In 3D-simulations, the computational spanwise length was six diameters. However, for $Re = 200$ and 250 a spanwise length of ten diameters was also investigated, with small to negligible effects on the global results.

The simulations indicate a stable 2D laminar shedding flow at $Re = 150$, whereas the effects of three-dimensional flow appear at $Re = 200$. Three-dimensional effects are more pronounced when the Reynolds number is increased, and using 2D-simulations led to a non-accurate prediction of flow structures and global quantities such as force coefficients and Strouhal number.

On consideration of the wake structure, A- and B-modes of secondary vortices are found, in similarity with the flow around circular cylinders. However, in seeming contrast to circular cylinders, the transitional flow around a square cylinder exhibits a phenomenon of low-frequency force pulsations ($Re = 200 - 300$).

For $Re = 200, 250$ and 300 (3D-simulations), the forces on the cylinder exhibited a marked and characteristic pulsation in time. The instants of maximum force level appeared to be random in time, although, for $Re = 200$ and 250, there seemed to be a preference for a pulsation rate corresponding to 10-16 mean shedding periods (60-100 time units). Associated with the presence of force pulsations was a time-shifted positive coupling between the instantaneous shedding frequency and the lift amplitude, with the shedding frequency leading the amplitude. Within the time regions of high force levels, the flow was in an ordered state with relatively small spanwise variations, whereas, within low-force regions, the three-dimensional effects were strong with a seemingly chaotic spanwise flow structure. The pulsating forces were closely related to the activity of the secondary vortices. Vortical structures similar to the mode A wake instability, as found in flow around circular cylinders, were present, especially in connection with the high-force regions. The spanwise wavelength of these instabilities were predominantly between 2 and 4 diameters. For $Re \geq 250$, structures similar to the mode B wake instability, with a dominant wavelength of about one diameter, were also present.

For $Re \geq 300$, the indicated spanwise coupling of lift forces increased with increasing Re. In particular, an extremely high spanwise correlation of lift forces was indicated for $Re = 500$.

Two-dimensional simulations for $Re \geq 300$ exhibited a period-doubling scenario of wake transition. Period-doublings were not present in the three-dimensional simulations.

The 2D results for mean drag were in reasonable agreement with experiments (see Fig. 10), although other quantities and flow characteristics for $Re \geq 200$ were primarily in sharp contrast to available experimental data and with the present 3D results. When considering blockage effects and experimental uncertainties the 3D results were in general agreement with experimental data (available only for Strouhal number and mean drag), see e.g. Figs. 10 and 11.

Some dissimilarities with the flow around a circular cylinder were noted.

6.5 Paper 5

This paper reported Large Eddy Simulation (LES) of the flow around a square cylinder at $Re = 22 \times 10^3$. Three different subgrid scale models, the Smagorinsky, the dynamic and a dynamic one-equation model, were applied.

The study computed some global quantities, such as the dominating wake frequency (Strouhal number) and the mean and RMS values of lift and drag. A series of time-averaged resolved velocities, pressure and turbulent stresses were provided for comparison of the numerical results with experimental results. This study shows that the dynamic model predicts the lowest level of all components of Reynolds stresses of the three models. It also predicts higher pressure in the wake region. Thus, it is concluded that the lower Reynolds stresses correspond to higher pressure region in the wake flow which leads to lower drag forces in this model. It is also observed that the dynamic model produces more wiggles upstream of the body than do the other models. These extra wiggles are caused by numerical problems associated with the negative values and

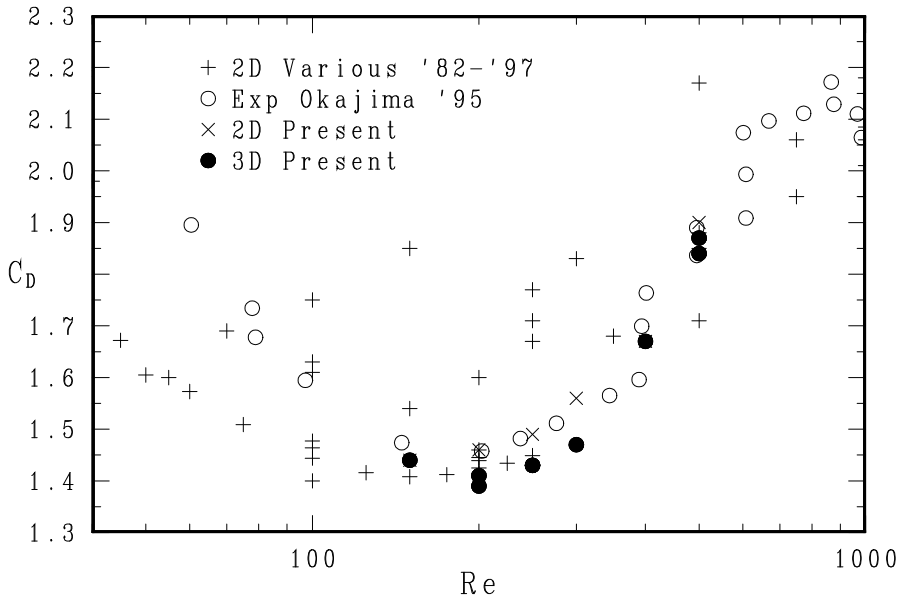

Figure 10: Mean drag coefficient *vs.* *Re*.

large variation in the dynamic coefficient.

In spite of the fact that the CPU time for each iteration in the case of the one-equation model is higher than for the dynamic model, the CPU required time at each time step is higher for the dynamic model. This is a result of numerical problems associated with this model, which increase the number of iterations needed for convergence at each time step.

By taking consideration to computed global quantities, mean flow and comparisons of present results with experiments, this simulation shows that the results produced by the dynamic model differ relative to the other models. This study also shows that the one-equation subgrid-scale model gives the best agreement with experiments than the other two models.

Back scattering was observed in the shear layer, close to the upstream as well as in a small region also close to the downstream corners of the body for the one-equation model.

7 Concluding Remarks and Recommendations for Future Work

The main objectives of this thesis work have been, for incompressible flow around single rectangular cylinders, (i) to partly fill the considerable gap of knowledge concerning the effects of body aspect ratio, flow incidence and blockage at low to moderate Reynolds numbers, and (ii) to further investigate the vortex shedding process and its related wake transitional phenomena, in particular for the square cylinder at zero incidence. The problem under consideration has four fundamental physical parameters: the Reynolds number, Re (based on an appropriate cross dimension, e.g. the projected width d), the body aspect ratio, B/A (where B is the longest side), the flow incidence angle (or angle of attack), α, and, finally, the blockage ratio, β (ratio between

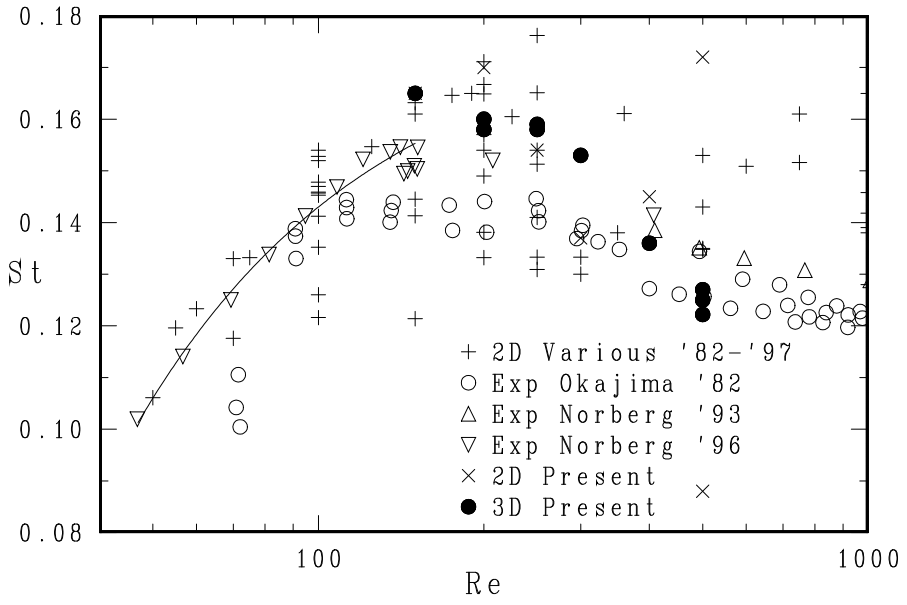

Figure 11: Strouhal number *vs.* Re. The solid line corresponds to $St = 0.18 - 3.7/Re$, as suggested from the laminar shedding data of Norberg 1996.

body width d and distance between confining walls). Given the limitations on computer resources, the philosophy was that the predictions should be as accurate and reliable as possible, especially for the forces acting on the cylinder. Although the work was not exhaustive in all physical parameters, it is nevertheless believed that the above objectives have been fulfilled. However, as with most scientific work, some questions have been answered but perhaps even more questions have emerged during the course of study, which calls for a further investigations. Examples of unanswered questions remaining from this work are given below. For brevity, as in Paper 4, the flow around a square cylinder at zero incidence is abbreviated as SC-flow.

1. By using the linearized Stuart-Landau equation, the actual onset of vortex shedding for flow around a square cylinder at incidence was investigated. Within the full range of possible incidences, $0^o \leq \alpha \leq 45^o$, the simulations indicated the onset to occur within the interval of $40 < Re_{cr} < 55$ ($\beta = 5\%$). Some questions for further work are:

   (a) What are the onset Re for other rectangular sections and for various flow incidences? For instance, given a certain limited body aspect ratio, what are the minimum and maximum onset Reynolds numbers?

   (b) What is the true influence of blockage on the critical Reynolds number for onset of vortex shedding? It is worth mentioning, for SC-flow, that, from a numerical linear stability analysis at a blockage of $\beta = 14.2\%$, Kelkar & Patankar [6] report $Re_{cr} = 53$ whereas, in the practically zero blockage experiments of Norberg [18], the critical value is estimated to be within $Re_{cr} = 47 \pm 2$. As the present investigation at $\beta = 5\%$ gave

$Re_{cr} = 51.2 \pm 1.0$ ($\alpha = 0^o$), it may be conjectured that the critical Reynolds number increases with increasing blockage.

(c) Were the present predictions of critical Reynolds numbers for onset of vortex shedding affected by the type of outlet boundary condition, size of calculation domain and the far-field resolution?

For SC-flow, with a far-field resolution of $\Delta = 0.7$ and when using NBC at outlet, the critical onset value was $Re_{cr} = 52.0$ as compared with $Re_{cr} = 51.2$ when using CBC with $\Delta = 0.5$. The numerical parameters were otherwise the same. It is unclear whether this discrepancy is dependent most on different outlet boundary conditions or on a difference in Δ.

The onset of vortex shedding occurs when a sufficiently large portion of the near wake becomes absolutely unstable [10]. In this respect, the development of near wake velocity profiles have a direct relation to the degree of (absolute) instability. It may be that the most efficient way of determining onset conditions is a combination of numerical simulations and laboratory experiments and making use of advanced stability analysis [5].

2. From this study, at a blockage ratio of 5.6% and for SC-flow, it was indicated that the transition from 2D to 3D flow occurs within the interval between $Re = 150$ and $Re = 200$. The 3D-simulation at $Re = 150$ did not exhibit any sign of spanwise variation i.e. the flow was completely two-dimensional. The low-blockage experiments carried out for an aspect ratio of 200 by Norberg [18] indicated that the transition from 2D- to 3D-flow occurs at around $Re = 150$. Although it was not possible from the present numerical simulation to obtain the exact critical Reynolds number at which this transition occurs there are some points that need further elucidation. For example:

   (a) For SC-flow, what is the true critical Reynolds number for the onset of three-dimensional flow? What is the influence of blockage?

   (b) How is this critical Reynolds number affected by spatial/time resolutions and the computational spanwise aspect ratio, A ?

   (c) What is the influence of body side ratio and flow incidence on this transitional behavior?

3. From this study on SC-flow, an extremely high correlation of lift forces was indicated for $Re = 500$ (A=6). For all other cases at $Re \geq 200$, except $Re = 500$, the RMS lift from 2D simulations was also significantly higher than those from 3D simulations. The seemingly good prediction of RMS lift from a 2D simulation and high correlation of lift forces for $Re = 500$ is actually an indication that a longer aspect ratio might be needed for the simulation to be reliable. Thus, at least for $Re = 500$, accurate simulations for $A > 6$ are needed.

4. In turbulent SC-flow, i.e. for approximately $Re > 200$, measured data (Okajima & Sugitani [14]) and unpublished results by Norberg reveal that the base suction coefficient ($-C_{pb}$) increases to a local maximum at around $Re = 2 \times 10^3$, where $-C_{pb} \approx 1.55$. This corresponds to an indicated maximum drag coefficient of about 2.25 ($C_D \approx -C_{pb} + 0.7$ [12]). At around $Re = 2 \times 10^3$ there is also a local minimum in the Strouhal number ($St \simeq 0.125$, see [12]). Between $Re = 200$ and 2×10^3, approximately, there is a trend of increasing C_D, $-C_{pb}$ and $(St)^{-1}$. In SC-flow, what is happening at about this apparent critical Re of about 2×10^3? The above trend is completely opposite to the flow around a circular cylinder, for which there instead is a minimum in C_D, $-C_{pb}$ and $(St)^{-1}$ at around $Re = 1.5 \times 10^3$ [13]. The reasons for this discrepancy between SC-flow and the flow around a circular cylinder are unclear. More investigations are needed.

5. Except for Paper 5, which is for SC-flow at $Re = 22 \times 10^3$ using LES, investigations on the influence of various computation parameters were performed ($Re \leq 500$). In many cases, by using the RMS lift and drag coefficients as indicators, the results were found to be dependent on such parameters. When using only the Strouhal number and/or the mean drag coefficient some of these numerical effects did not show up correctly. A question is now propounded. For the LES-simulations as presented in Paper 5, what are the remaining effects of spatial/time resolutions and computational domain sizes, especially the spanwise dimension?

References

[1] P. W. Bearman and D. M. Trueman. An investigation of the flow around rectangular cylinders. *Aeronautical Quarterly*, 23:229 – 237, 1972.

[2] R.D. Blevins. *Flow-Induced Vibration.* Van Nostrand Reinhold, New York, 1990.

[3] L. Davidson and B. Farhanieh. CALC-BFC: A finite-volume code employing collocated variable arrangement and cartesian velocity components for computation of fluid flow and heat transfer in complex three-dimensional geometries. Rept. 92/4, Thermo and Fluid Dynamics, Chalmers University of Technology, Gothenburg, 1992.

[4] R. Franke, W. Rodi, and B. Schönung. Numerical calculation of laminar vortex-shedding flow past cylinders. *J. Wind Engng Ind. Aero.*, 35:237–257, 1990.

[5] C. P. Jackson. A finite-element study of the onset of vortex shedding in flow past variously shaped bodies. *J. Fluid Mech.*, 182:23–45, 1987.

[6] K. M. Kelkar and S. V. Patankar. Numerical prediction of vortex shedding behind a square cylinder. *Int. J. Num. Meth. Fluids*, 14(3):327–341, 1992.

[7] B. Van Leer. Towards the ultimate conservative difference scheme. Monotonicity and conservation combined in a second order scheme. *Journal of Computational Physics*, 14:361–370, 1974.

[8] B. Van Leer. Towards the ultimate conservative difference scheme. V. A second-order sequel to godonov's method. *Journal of Computational Physics*, 32:101–136, 1979.

[9] B.P. Leonard. A stable and accurate convective modeling based on quadratic upstream interpolation. *Comp. Meth. Appl. Mech. Eng.*, 19:59–98, 1979.

[10] P. A. Monkewitz. The role of absolute and convective instability in predicting the behavior of fluid systems. *Eur. J. Mech., B/Fluids*, 9(5):395–413, 1990.

[11] Y. Nakamura, Y. Ohya, S. Ozono, and R. Nakayama. Experimental and numerical analysis of vortex shedding from elongated rectangular cylinders at low Reynolds numbers 200 to 1000. In *Proc. EECWE '94, Warzaw, July 1994*, pages 1 – 9, 1994.

[12] C. Norberg. Flow around rectangular cylinders: pressure forces and wake frequencies. *J. Wind Engng Ind. Aero.*, 49:187–196, 1993.

[13] C. Norberg. An experimental investigation of the flow around a circular cylinder: influence of aspect ratio. *J. Fluid Mech.*, 258:287 – 316, 1994.

[14] A. Okajima and K. Sugitani. Strouhal number and base pressure coefficient of a rectangular cylinder. *Trans. JSME, Ser. B*, 50(459):2004–2012, 1984.

[15] S.V. Patankar. *Numerical Heat Transfer and Fluid Flow.* McGraw-Hill, New York, 1980.

[16] M. Provansal, C. Mathis, and L. Boyer. Bénard-von Kármán instability: transient and forced regimes. *J. Fluid Mech.*, 182:1–22, 1987.

[17] A. Roshko. On the development of turbulent wakes from vortex streets. Report 1191, NACA, 1954.

[18] A. Sohankar, C. Norberg, and L. Davidson. Numerical simulation of unsteady low-Reynolds number flow around a rectangular at incidence. *J. Wind Engng Ind. Aero.*, 69-71:189–201, 1997.

[19] A. Sohankar, C. Norberg, and L. Davidson. Low-Reynolds flow around a square cylinder at incidence: Study of blockage, onset of vortex shedding and open boundary condition. *Int. J. Num. Meth. Fluids*, 26:39–56, 1998.

[20] N. Stegell and N. Rockliff. Simulation of the effects of body shape on lock-in characteristics in pulsating flow by the discrete vortex method. In *The 3rd Int. Colloquium on Bluff Body Aerodynamics & Applications*, Virginia Polytechnic Institute and State University, 1996.

[21] V. Strouhal. Über eine besondere Art der Tonerregung. *Ann. Physik und Chemie, Neue Folge*, 5:216–251, 1878.

[22] S. Taneda. Experimental investigation of the wakes behind cylinders and plates at low Reynolds numbers. *J. Phys. Soc. Japan.*, 11:302, 1956.

[23] J. F. Thompson, Z.U.A. Warsi, and C. W. Mastin. *Numerical Grid Generation; Foundations and Applications*. Elsevier Science, 1985.

[24] M. M. Zdravkovich. *Flow Around Circular Cylinders*. Oxford Science Publications, 1997.